Soy-lignin Bonded *Rhizophora* spp. as a Bio-based Phantom: Impact of Adhesives on Attenuation

Usha R. Baskaran,[a] Saadiatul Nur Aqilah Mohd Zakaria,[a] Siti Hajar Zuber ,[a,*] Muhammad Fahmi Rizal Abdul Hadi,[b] Nurul Ab. Aziz Hashikin,[b] and Muhammad Safwan Ahmad Fadzil [a]

The feasibility of utilising soy-lignin bonded *Rhizophora* spp. wood was investigated as a sustainable, bio-based phantom material for radiation dosimetry applications. Various samples with differing thicknesses and adhesive compositions were prepared to evaluate the consistency and reliability of the material's attenuation properties. The experimental assessment was conducted using two standard gamma-emitting radioisotopes, Cobalt-60 and Cesium-137, to encompass a range of photon energies relevant to medical radiation applications. Monte Carlo simulations were performed using the GATE platform to compute the linear and mass attenuation coefficients. The study evaluates the impact of adhesives on attenuation behaviour. The lowest overall attenuation variation of 0.06 to 1.40% was observed in the soy–lignin bonded *Rhizophora* spp. at a particle size of 104 to 210 µm with the addition of 6 and 12% adhesives, suggesting that changes in adhesive content do not appreciably affect the attenuation behaviour, demonstrating its potential as a bio-based phantom material in radiation study.

DOI: 10.15376/biores.21.2.3394-3416

Keywords: Rhizophora spp.; Attenuation coefficient; Monte Carlo; GATE; Phantom; Bio-based

*Contact information: a: Centre for Diagnostic, Therapeutic and Investigative Studies, Faculty of Health Sciences, Universiti Kebangsaan Malaysia, 50300, Kuala Lumpur, Malaysia; b: School of Physics, Universiti Sains Malaysia, 11800, Penang, Malaysia; *Corresponding author: hajarzuber@ukm.edu.my*

INTRODUCTION

Mangrove trees of the genus *Rhizophora* spp. are key components of coastal, tropical, and subtropical sedimentary ecosystems (Stocken *et al.* 2022). *Rhizophora* spp. grows in Malaysia's coastal tidal plains, and with the country being the third-largest mangrove holder, the species is readily accessible for research purposes (Zuber *et al.* 2020). Since the 1980s (Zuber *et al.* 2021b; Tousi and Sadeghi 2024), mangrove wood has been extensively regarded as a phantom material due to its special qualities, including renewability, biodegradability, low toxicity, availability, low cost, and ease of fabrication. Additionally (Zuber *et al.* 2021a; Tousi and Sadeghi 2024), the density of wood closely approximates that of human tissues and water, rendering it highly suitable for use as a tissue-equivalent phantom material. *Rhizophora* spp. was first identified as a potential phantom material in a study by Sudin *et al.* (1988). Since then, growing research interest has focused on evaluating the suitability of natural wood as a phantom material capable of simulating the interaction of human soft tissue with ionising radiation (Bradley *et al.* 1991; Sudin *et al.* 1988). In these studies, twenty-five different wood species were investigated in terms of mass density and photon attenuation properties to assess their compliance with

soft tissue equivalency requirements. The findings demonstrated that *Rhizophora* spp. possesses an optimal mass density of approximately 1040 kg·m^{-3}, with effective linear and mass attenuation coefficients at a photon energy of 59.54 keV. These encouraging results prompted further investigations into the radiographic imaging and scattering characteristics of *Rhizophora* spp. (Tajuddin *et al.* 1996). Furthermore, raw *Rhizophora* spp. also demonstrates excellent scattering and radiographic properties (Tousi and Sadeghi 2024).

In radiation studies, a phantom is a specially designed object that mimics the radiation absorption and scattering properties of human tissue, playing a crucial role in the development, dosimetry (Zuber *et al.* 2021a; Abdi *et al.* 2025; Khoshhal and Torshabi 2024), and quality assurance of imaging and therapeutic procedures. Phantoms allow for safe and repeatable experiments without exposing patients to unnecessary radiation, making them indispensable for dosimetry calibration, treatment planning verification, and imaging system evaluation. They are used to simulate various anatomical regions, ensuring accurate dose delivery and image quality. The importance of phantoms lies not only in their ability to improve clinical safety and precision but also in supporting the advancement of new radiation technologies through consistent and ethical testing frameworks.

Phantom materials are artificial alternatives with similar mass attenuation coefficients and effective atomic numbers that are intended to mimic human tissues. Phantoms can be fabricated from a wide range of materials, including polymers, gels, plastics, and biological tissues. In medical physics (Buyukyildiz *et al.* 2024), phantoms are widely used to mimic radiation interactions with human tissues in both therapeutic and diagnostic imaging applications. In radiotherapy, phantoms are used for device calibration and performance evaluation, pre-treatment dose estimation, image quality assessment in modalities such as magnetic resonance imaging (MRI), computed tomography (CT), positron emission tomography (PET), and the development and validation of radiation treatment plans.

Phantoms are essential in radiological imaging because they replicate the behavior of human tissues and organs, accurately reflecting their physical and radiological properties for scientific research. Therefore, selecting appropriate materials is crucial to guarantee that a phantom functions as intended (Khallouqi *et al.* 2024; Almalki *et al.* 2024). Previous literature reported the assessment of epoxy and polyester resins as substitutes for polymethyl methacrylate (PMMA) in CT dosimetry phantoms (Khallouqi *et al.* 2024). GEANT4/GATE simulations were used to calculate the mass attenuation coefficients. The findings show that polyester resin has radiological characteristics more similar to PMMA. According to another publication, gelatin samples were prepared with densities in range from 1.04 to 1.08 g·cm^{-3}, closely matching human tissue (Almalki *et al.* 2024). Comparison with XCOM breast tissue data indicated higher gelatin concentrations suitable for breast tissue simulation.

Another study presented the simulations of γ-ray transmission through tissue-equivalent solid phantoms using medical radionuclide sources, ^{99m}Tc, ^{131}I, ^{137}Cs, and ^{60}Co (Moradi *et al.* 2019). The results show that transmitted photon spectra for water, soft tissue, breast, brain, and lung phantoms are largely independent of material composition, whereas bone exhibits distinct spectral differences, primarily due to density effects. Previous literature also reported the water equivalency of several solid phantom materials, A-150, PMMA, Polystyrene, Solid Water (RMI 457), Solid Water (RW3), Virtual Water, Solid Water (WT1) and Water Equivalent (Wte) solid phantoms, and these samples were investigated by calculating kerma coefficients (Abdi *et al.* 2025). Solid Water (RMI 457) was identified as the most optimal material, confirming its applicability in radiology and

radiotherapy quality assurance.

To ensure consistency and accuracy in radiation dose delivery, quality assurance (QA) procedures are conducted using phantoms that mimic the human body. These tests assess radiation attenuation (Zuber *et al.* 2022a, 2024a,b), dose distribution, and image accuracy. However, the choice of phantom material is crucial, as it affects attenuation coefficient consistency and may introduce impurities, increasing uncertainties. Recent studies explore the development and comparison of solid and water-based solid phantoms, but practical challenges and potential invalid results make their creation difficult. Consequently, plastic-based solid phantoms, such as the RANDO and ATOM phantom, which is made from Perspex, continue to be widely used in radiotherapy, even though they are often criticised for being non-personalised, expensive, and not easily accessible (Scalzetti *et al.* 2008; Silberstein and Sun 2024). Previous literature reported that while some materials have optimal properties as phantoms, others such as high-density polyethylene (HDPE) differ significantly, which can lead to inaccuracies in dose delivery if not carefully considered (Kanematsu *et al.* 2013).

Recent studies involving the use of natural materials have shown encouraging results, and there are continuing efforts to explore their potential as viable alternatives (Marashdeh *et al.* 2012; Yusof and Fahmi 2017; Yusof *et al.* 2018, 2017; Abd Hamid *et al.* 2018; Samson *et al.* 2020a,b,c, 2023; Zuber *et al.* 2020, 2022b, 2025). *Rhizophora* spp. has gained interest due to its physical and radiological properties, which are similar to human tissue. An article states that powdered *Eremurus* spp. root was used as a bio-based adhesive to bond *Rhizophora* spp. particleboard samples at two treatment levels, 6% and 12%. The simulated and theoretical mass attenuation coefficients of all the particleboards closely matched those of young breast tissue, consistent with previous experimental findings. The effective atomic number (Z_{eff}) of the *Rhizophora* spp. particleboard phantom is increased by adding powdered *Eremurus* spp. root as a bio-based adhesive (Tousi *et al.* 2022). Thus, apart from consideration of the characteristics displayed by the phantom, the adhesive of the material binding also needs to be considered to prevent impurity formation within the phantom.

Monte Carlo GATE (Buvat and Lazaro 2006; Thiam *et al.* 2008; Grevillot *et al.* 2011; Jan *et al.* 2011; Sadoughi *et al.* 2014; Sarrut *et al.* 2022, 2014; Benameur *et al.* 2023; Nasr *et al.* 2024), including the GATE 4 version, is a highly reliable tool in medical physics and radiation studies. It is known for its ability to precisely simulate how particles interact with complex structures in the body. Its biggest strength lies in its accuracy, with studies showing it can calculate doses within 1% of actual measurements, while other systems may have deviations of 3% to 5%, making GATE a trusted choice for radiation studies (Park *et al.* 2021). According to a previous literature, it was demonstrated that the linear and mass attenuation coefficients of soy - lignin bonded *Rhizophora* spp. particleboard at low photon energies, as determined by GATE simulations, were in close agreement with the experimental measurements, with the smallest deviation being 0.3%. Overall, the results indicate good consistency between the simulation and experimental data, demonstrating GATE as an appropriate tool for validating attenuation coefficient measurements of bio-based phantom materials for application in medical physics (Zuber *et al.* 2024a).

This work evaluated the mass attenuation coefficient of phantom material at different percentages of adhesives using Monte Carlo GATE. The attenuation coefficient was determined by analysing different *Rhizophora* spp. samples with varying elemental compositions. The consistency and reliability of the calculated attenuation coefficients were evaluated using ^{60}Co and ^{137}Cs gamma-ray sources.

MATERIAL AND METHODS

In this work, particleboards were fabricated using *Rhizophora* spp. wood, incorporating three different percentages of soybean flour and lignin as an adhesive mixture. *Rhizophora* spp. wood was collected from a mangrove factory in Perak. The wood trunk was dried and cut into a smaller size using a saw machine. Then, the wood was ground onto smaller particles which later sieved into three different particle sizes. The wood particles were dried before they were mixed with adhesive. For adhesive, soybean flour (type I) and lignin (alkali, low sulfonate content) in powder form were purchased from Sigma Aldrich, Germany, and used as received. For the fabrication process, the particleboards were prepared by using hot pressing at approximately 200 °C, with pressure of 20 MPa for about 20 minutes at a target density of 1 g·cm^{-3}. The adhesives were prepared according to the calculation as shown in Eq. 1,

$$\rho = \frac{M}{V};\ \rho_t = 1 g cm^{-3}$$
$$M_R = W_R\% \times \rho V \times (1 + MC_R\%)$$
$$M_S = W_S\% \times \rho V \times (1 + MC_S\%)$$
$$M_L = W_L\% \times \rho V \times (1 + MC_L\%)$$
$$M_W = 7\% \times \rho V - [\,(M_R \times MC_R\%) + (M_S \times MC_S\%) + (M_L \times MC_L\%)\,] \quad (1)$$

where ρ, M, and V are density (g·cm^{-3}), mass (g), and volume (cm^3) of the particleboard, respectively. Parameters M_R, W_R%, and $MC\%_R$ are the approximate mass (g), weight percentage (%), and moisture content (%L) of *Rhizophora* spp. powder. The parameters M_S, W_S%, and $MC\%_S$ are the approximate mass (g), weight percentage (%), and moisture content (%L) of soybean flour. Parameters M_L, W_L%, and $MC\%_L$ are the approximate mass (g), weight percentage (%), and moisture content (%L) of lignin. Parameter M_W is the approximate mass (g) of saline water. Table 1 lists the fractional weight of *Rhizophora* spp., whereas Table 2 records the particle size and adhesive content for each sample. Table 3 lists the particleboard manufacturing condition.

Table 1. Fractional Weight of *Rhizophora* spp.

Composition	Chemical formula	Fractional weight of the composition, w_i
Sodium oxide	Na_2O	0.06777
Magnesium oxide	MgO	0.03056
Aluminium oxide	Al_2O_3	0.00303
Silicon dioxide	SiO_2	0.01414
Phosphorus pentoxide	P_2O_5	0.01095
Sulfur trioxide	SO_3	0.03501
Chlorine	Cl	0.19607
Potassium oxide	K_2O	0.04936
Calcium oxide	CaO	0.53794
Manganese (II) oxide	MnO	0.01262
Iron (III) oxide	Fe_2O_3	0.02873
Bromine	Br	0.00273
Strontium oxide	SrO	0.00868
Bismuth (III) oxide	Bi_2O_3	0.00238

Table 2. Particle Size and Adhesive Content for Each Sample

Sample	Particle size (µm)	Adhesive content (%)
A0	211 to 500	0% Soy flour and Lignin
A6	211 to 500	4.5% Soy flour and 1.5% Lignin
A12	211 to 500	9% Soy flour and 3% Lignin
B0	104 to 210	0% Soy flour and Lignin
B6	104 to 210	4.5% Soy flour and 1.5% Lignin
B12	104 to 210	9% Soy flour and 3% Lignin
C0	0 to 103	0% Soy flour and Lignin
C6	0 to 103	4.5% Soy flour and 1.5% Lignin
C12	0 to 103	9% Soy flour and 3% Lignin

Table 3. Particleboard Manufacturing Condition

Information	Condition
Raw Material	*Rhizophora* spp.
Moisture Content	1.39 to 8.87 (%/L)
Particleboard Size	23.0 × 23.0 × 0.5 (cm^3)
Target Density	1.0 ($g \cdot cm^{-3}$)
Adhesive	Soy flour; lignin
Hot Pressing Conditions	Temperature: 200 (°C) Time: 20 (min) Pressure: 20 (MPa)

This work is a simulation study that measures the potential of bio-based *Rhizophora* phantom through the consistency of the mass attenuation coefficient and uncertainties measurement for the impurity presence using Monte Carlo GATE. GATE was used to measure the linear and mass attenuation coefficient of the phantom material using two different sources, ^{137}Cs was evaluated at its principal photon energy of 0.662 MeV, while ^{60}Co was analysed using an effective photon energy of 1.25 MeV. A total of nine samples with different elemental compositions were analysed through X-ray fluorescence (XRF; Panalytical Axios Max; PANalytical, Malvern, UK) analysis using the Omnian method from the Centre for Global Archeological Research Earth Material Characterisation Laboratory, Universiti Sains Malaysia. The elemental composition data is included in Appendix A as supplementary data.

For Monte Carlo GATE, a custom-built personal computer (PC) with INTEL Core I9 14900K 24 Cores, 32 Threads, and a 3.2 GHz LGA1700 Processor was utilised with an Ubuntu 22.04.4 LTS operating system (OS). GATE v9.4 including the Geant4 v11.2.1 and Root v6.28/12 platforms were used in this simulation work to generate the geometry of the energy transmission experimental setup. However, to ensure the code can be run anytime without using the main PC, the usage of TeamViewer and Anydesk application acted as a remote system to obtain the result and ease in conducting data analysis without requiring additional extension.

In this work, the thickness for every sample was set at 1.0964 cm, 2.0964 cm, 3.0964 cm, and 4.0964 cm, at 1.0 $g \cdot cm^{-3}$ target density, in *geometry.mac*. Two different sources (^{60}Co and ^{137}Cs) were used in this simulation study with specific energy spectrum listed in *source.mac* and *main.mac*. For this study, a number of 10^4 histories were used to run the simulation. Figure 1 illustrates the command script in *physics.mac*, whereas Fig. 2 lists the command script in *main.mac*.

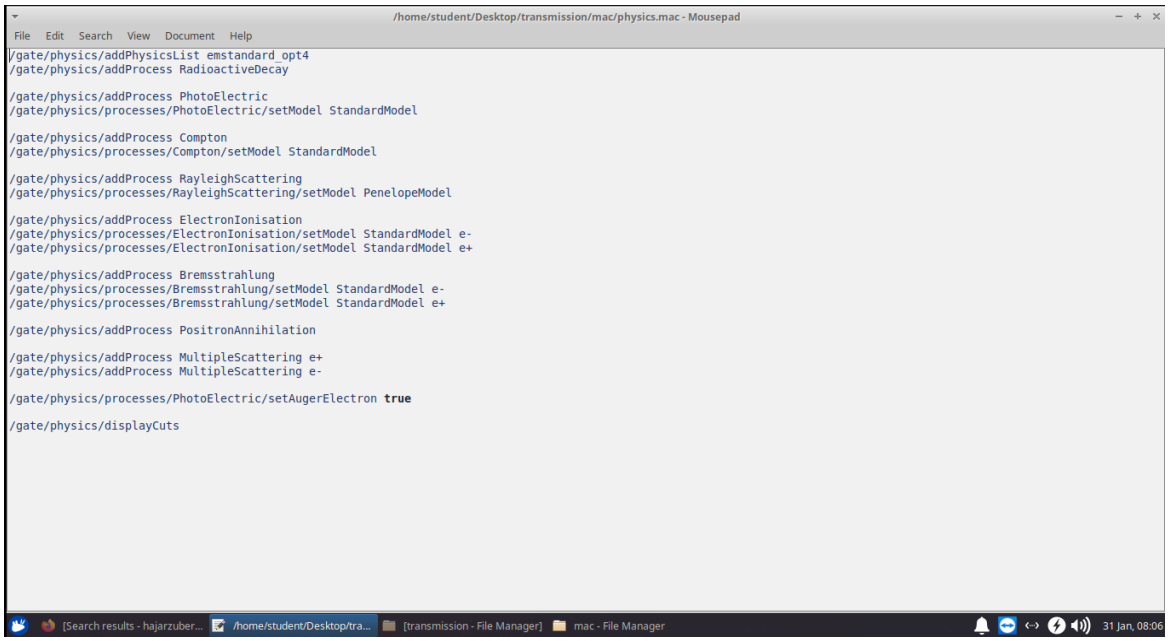

Fig. 1. The file of *physics.mac* that states the interaction in GATE

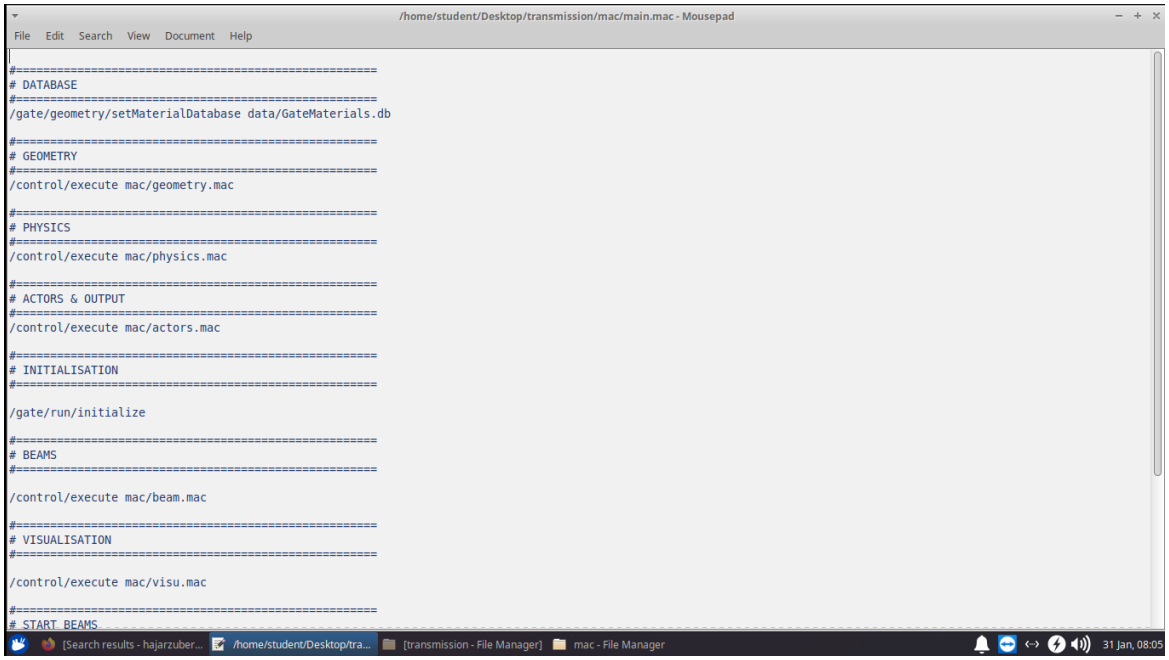

Fig. 2. The *main.mac* file that comprises the beam, materials, number of primaries, and the code for running visualisation, initialisation, and output

Upon updating the file and linking it to *main.mac*, the data were run using the command *Gate mac/main.mac*. The command read the *main.mac* script, which includes codes for the element samples, materials, and beam sources. These codes were executed through a terminal in the main transmission file to ensure proper detection of required or blocked codes. It also ensured that the results were recorded in an output file, which was further divided into detector and scattered detector data.

The presence of the scattered radiation and the amount of radiation directed from the source to the receptor could be displayed using the command of *Gate mac/main.mac* -

-qt. The data were analysed using the *detector.txt* file in the output, rather than the *detector scatter.txt* file, as the study focused on measuring the attenuation of ^{60}Co and ^{137}Cs sources through the sample. This process was repeated for each sample to determine the attenuation. Figures 3 through 5 illustrate the attenuation simulation and setup in GATE.

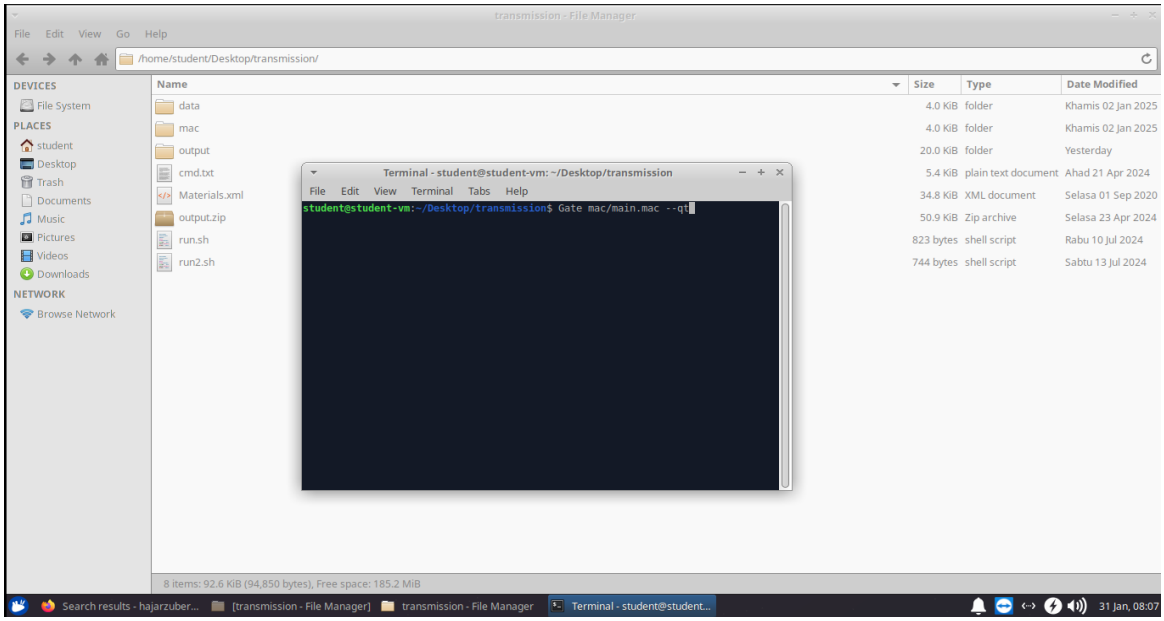

Fig. 3. The command *Gate mac/main.mac --qt* for visualisation

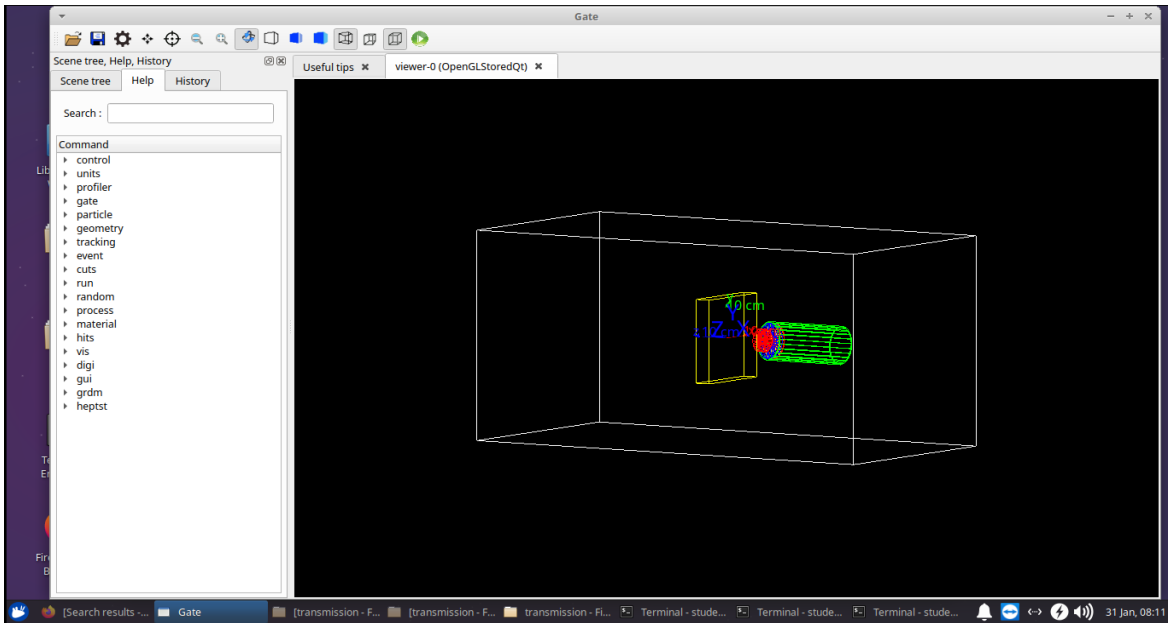

Fig. 4. The general attenuation setup in GATE

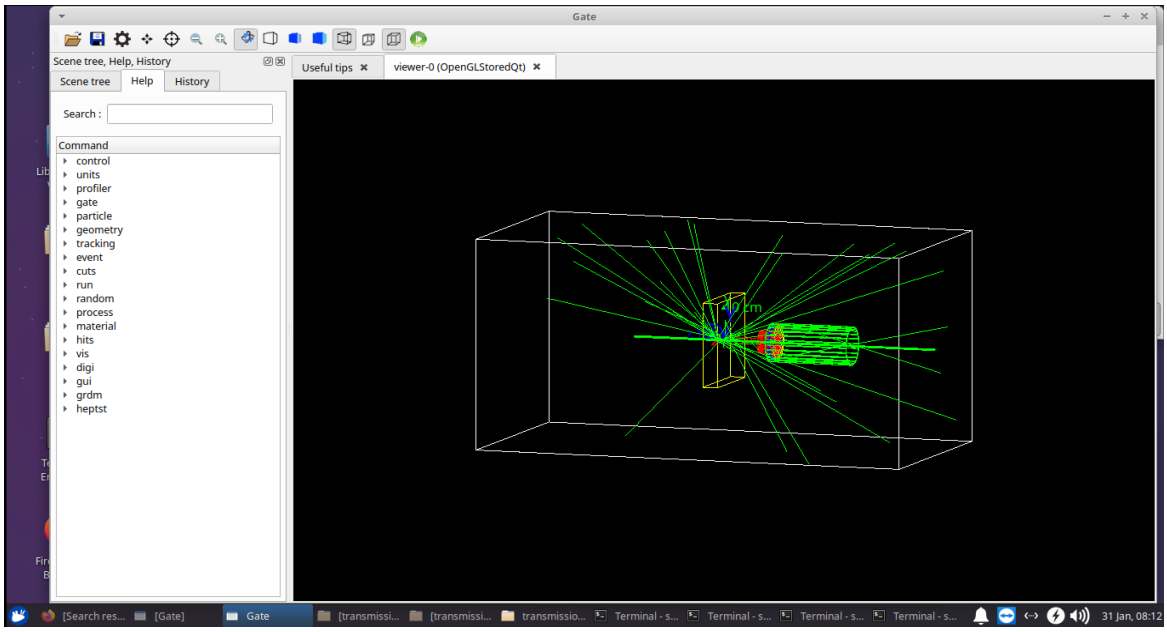

Fig. 5. The visualisation of the setup using sample A0 for the thickness of 4.0964 cm using ^{60}Co

The photon attenuation properties of the samples were analysed using the Beer-Lambert law. Based on the results, the data for each sample and source were plotted on a graph for the calculation of the linear attenuation coefficient using Eq. 2,

$$I = I_0 e^{-\mu x} \tag{2}$$

where I_0 and I are the incident and transmitted photon intensities (count per second), μ (cm^{-1}) is the linear attenuation coefficient of the material, and x is the thickness (cm) of the samples. This principle forms the basis for evaluating the gamma ray shielding effectiveness of materials (Kaya 2025; Abdalla *et al.* 2022). To account for material density, the density-independent mass attenuation coefficient $(\mu/\rho, cm^2/g)$ was employed:

$$I = I_0 e^{-(\mu/\rho)\rho x} = I_0 e^{-(\mu/\rho)d} \tag{3}$$

In Eq. 3, d is the thickness that represented in the material's unit area mass (g/cm^2). For composites containing multiple elements or compounds, the effective mass attenuation coefficient was calculated using the mixture rule:

$$\mu/\rho_{composite} = \sum_i w_i (\mu/p)_i \tag{4}$$

where w_i denotes the weight fraction of the i^{th} component and $(\mu/p)_i$ is the mass attenuation coefficient, which can be determined from the relation,

$$w_i = \frac{a_i A_i}{\sum a_i A_i} \tag{5}$$

where A_i is the atomic weight and a_i is the number of atoms of element i in the compound. The effective atomic number (Z_{eff}) of the sample was calculated as:

$$Z_{eff} = \frac{\sum f_i A_i (\mu/p)_i}{\sum \frac{f_i A_i}{Z_i} (\mu/p)_i} = \frac{\sum f_i A_i Z_i}{\sum f_i A_i} \tag{6}$$

Finally, the half-value layer (HVL), representing the thickness required to reduce the incident radiation intensity by 50% was derived directly from the Beer-Lambert law:

$$HVL = \frac{0.693}{\mu} \quad (7)$$

Collectively, these expressions allow a complete assessment of gamma-ray attenuation in both pure and composite phantom materials, providing insight into their shielding efficiency.

RESULTS AND DISCUSSION

In this work, the results were compiled into a table to compare the consistency of linear and mass attenuation coefficients with the addition of different percentages of adhesives. Graphs of the mass attenuation coefficient *versus* sample thickness was plotted to examine the linearity of $ln(I_0/I)$ from the experiment, as shown in Figs. 6 and 7. Tables 4 and 5 record the linear and mass attenuation coefficient of samples using ^{60}Co and ^{137}Cs.

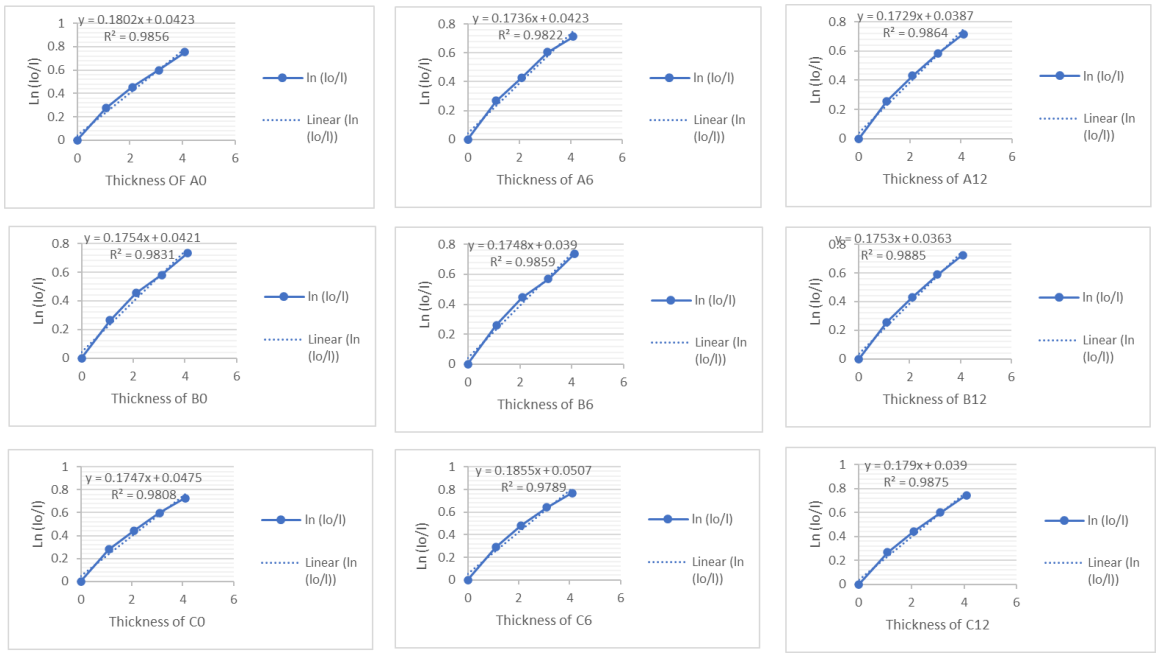

Fig. 6. The mass attenuation from all samples irradiated with ^{60}Co

The results indicate that samples A0 and C6 exhibited slightly higher mass attenuation coefficients (0.18 cm^2/g) compared to other samples (0.17 cm^2/g). The linear attenuation coefficients were consistent across all samples and closely followed the ideal $ln\ (I_0/I)$ relationship. Most graphs demonstrated strong linear correlations with R-values around 0.98, confirming reliable linearity. A minor deviation was observed for sample C6, with an R-value of 0.97, which did not significantly affect the overall trend. Slight slope variations were observed in samples A6, B0, and B6 at certain thicknesses, nevertheless, their deviations did not affect the overall consistency of the mass attenuation coefficient under ^{60}Co irradiation.

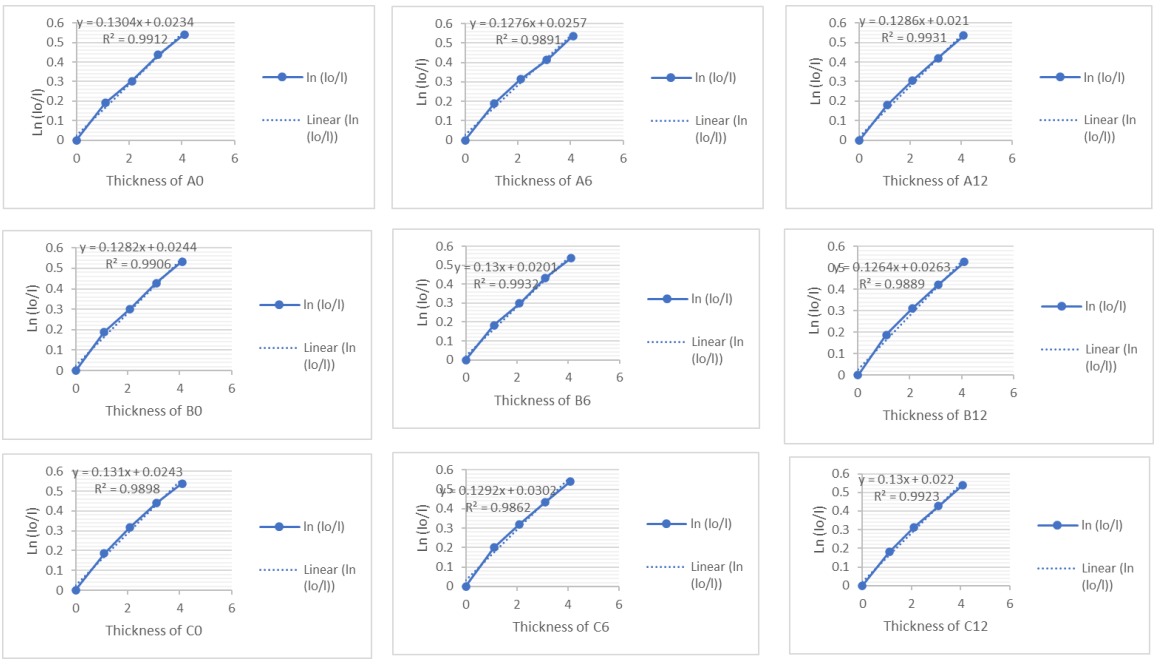

Fig. 7. The mass attenuation from all samples irradiated with ^{137}Cs

Table 4. Linear and Mass Attenuation Coefficient of Samples Using ^{60}Co

Sample	Thickness (cm)	Linear Attenuation Coefficient (μ) (cm^{-1})	Density, ρ (g/cm^3)	Mass attenuation Coefficient (μ/ρ) (cm^2/g)
A0	1.0964	0.1802	1.0	0.1802
	2.0964			
	3.0964			
	4.0964			
A6	1.0964	0.1736	1.0	0.1736
	2.0964			
	3.0964			
	4.0964			
A12	1.0964	0.1729	1.0	0.1729
	2.0964			
	3.0964			
	4.0964			
B0	1.0964	0.1754	1.0	0.1754
	2.0964			
	3.0964			
	4.0964			
B6	1.0964	0.1748	1.0	0.1748
	2.0964			
	3.0964			
	4.0964			
B12	1.0964	0.1753	1.0	0.1753
	2.0964			
	3.0964			
	4.0964			
C0	1.0964	0.1747	1.0	0.1747
	2.0964			
	3.0964			
	4.0964			

Sample	Thickness (cm)	Linear Attenuation Coefficient (μ) (cm^{-1})	Density, ρ (g/cm^3)	Mass attenuation Coefficient (μ/ρ) (cm^2/g)
C6	1.0964	0.1855	1.0	0.1855
	2.0964			
	3.0964			
	4.0964			
C12	1.0964	0.1790	1.0	0.1790
	2.0964			
	3.0964			
	4.0964			

A = 211 to 500 µm, B = 104 to 210 µm, C = 0 to 103 µm particle size ranges;
0 = 0% soy flour and lignin, 6 = 4.5% soy flour and 1.5% lignin, 12 = 9% soy flour and 3% lignin

Table 5. Linear and Mass Attenuation Coefficient of Samples Using ^{137}Cs

Sample	Thickness (cm)	Linear Attenuation Coefficient (μ) (cm^{-1})	Density, ρ (g/cm^3)	Mass Attenuation Coefficient (μ/ρ) (cm^2/g)
A0	1.0964	0.1304	1.0	0.1304
	2.0964			
	3.0964			
	4.0964			
A6	1.0964	0.1276	1.0	0.1276
	2.0964			
	3.0964			
	4.0964			
A12	1.0964	0.1286	1.0	0.1286
	2.0964			
	3.0964			
	4.0964			
B0	1.0964	0.1282	1.0	0.1282
	2.0964			
	3.0964			
	4.0964			
B6	1.0964	0.1300	1.0	0.1300
	2.0964			
	3.0964			
	4.0964			
B12	1.0964	0.1264	1.0	0.1264
	2.0964			
	3.0964			
	4.0964			
C0	1.0964	0.1310	1.0	0.1310
	2.0964			
	3.0964			

Sample	Thickness (cm)	Linear Attenuation Coefficient (μ) (cm^{-1})	Density, ρ (g/cm^3)	Mass Attenuation Coefficient (μ/ρ) (cm^2/g)
	4.0964			
C6	1.0964	0.1292	1.0	0.1292
	2.0964			
	3.0964			
	4.0964			
C12	1.0964	0.1310	1.0	0.1310
	2.0964			
	3.0964			
	4.0964			

A = 211 to 500 µm, B = 104 to 210 µm, C = 0 to 103 µm particle size ranges;
0 = 0% soy flour and lignin, 6 = 4.5% soy flour and 1.5% lignin, 12 = 9% soy flour and 3% lignin

The mass attenuation coefficients of samples A0, C0, and C12 were slightly higher (0.13 cm^2/g) than those of the other samples (0.12 cm^2/g). Overall, all samples had linear attenuation coefficients that closely matched the ideal ln (I_0/I) relationship. The graph demonstrated strong linear correlations with R-values ranging from 0.98 to 0.99. The slope appeared slightly steeper than the ideal linear graph in samples measured at thicknesses between 1.094 cm and 2.0964 cm; however, these minor deviations did not compromise the overall linearity or consistency of the mass attenuation coefficient under ^{136}Cs irradiation.

Based on Fig. 8, the mass attenuation coefficient using ^{60}Co at 1.25 MeV was presented in the higher range from 0.17 to 0.18 cm^2/g, while ^{137}Cs displayed a value with a range between 0.12 and 0.13 cm^2/g. Each of the samples displayed a consistent value that was within the range using respective sources. For the sample with a particle size of 211 to 500 µm (Sample A), the inclusion of adhesive resulted in disparities ranging from 1.38% to 4.05% compared with the formulation without adhesive. For the sample with a particle size of 104 to 210 µm (Sample B), the addition of adhesive led to smaller differences, ranging from 0.06% to 1.40%. In contrast, the sample with a particle size of 0 to 103 µm (Sample C) exhibited discrepancies between 0% and 6.18% upon the incorporation of adhesive, relative to the non-adhesive formulation. Among the three samples, Sample B (104 to 210 µm) demonstrated the lowest overall variation, indicating greater compositional stability and more uniform interaction between particles and adhesive. This demonstrates minimal disparity across different adhesive percentages, indicating that varying the adhesive percentage has a negligible effect on the attenuation.

To ensure the validity of the result, a comparison with a recent study was conducted that focuses more towards consistency of formation, material adhesive bonding, and impurity content. Previous literature reported the adhesion and purity of the material involving the attenuation consistency using an epoxy-based breast phantom at lower photon energy from 16.65 and 25.21 keV (Marashdeh and Abdulkarim 2023). The finding reported a slight increase in the linear attenuation coefficient with the addition of Carbopol 974p polymer. This increase may be attributed to the presence of different atomic numbers (Z) within Carbopol 974p, although μ and μ/ρ values did not change significantly with changes to the ratio of Carbopol polymer. The varying atomic numbers enhance the probability of photon interactions with gamma rays, thereby contributing to the observed rise in attenuation.

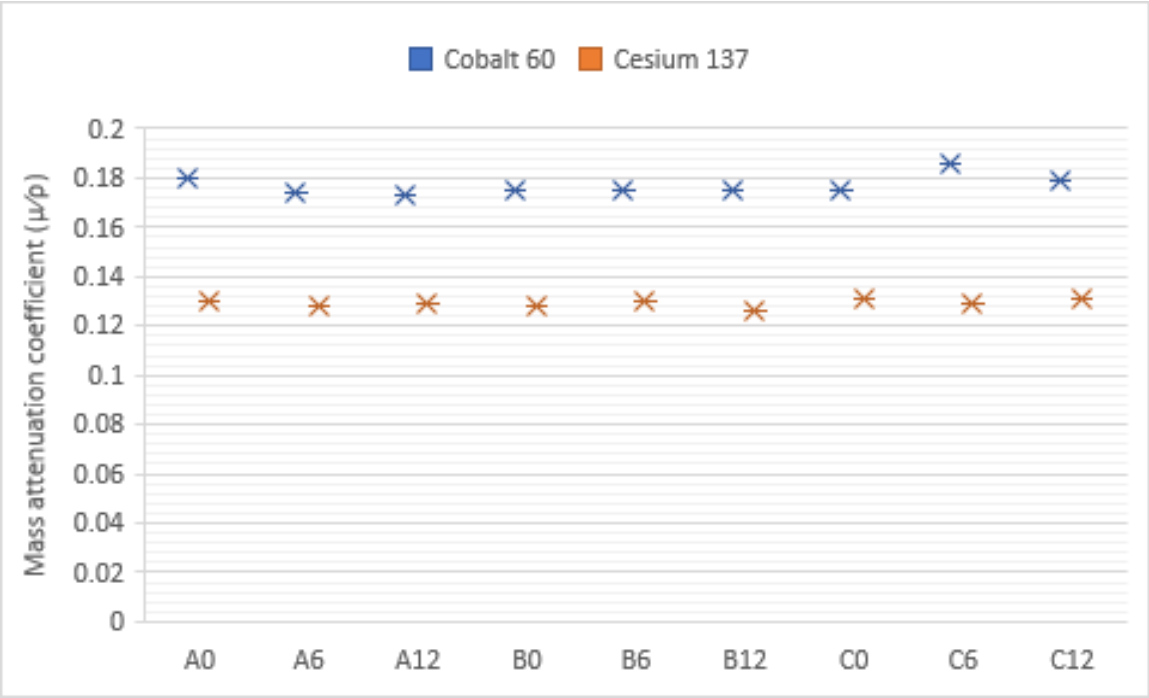

Fig. 8. The mass attenuation coefficient of all samples for both sources

Another article was reviewed based on tissue-equivalent material used in imaging and radiotherapy. A study conducted in 2020 focused on tissue-mimicking materials (TMM) and explored various modalities, including the latest machine developments and combinations like MRI with CT scans. The study concluded that the attenuation coefficient for tissue-mimicking materials generally falls within the range of 0.14 to 0.18 cm^2/g (McGarry *et al.* 2020). Building on these results, the consistency in attenuation coefficients observed here shows that the changes in adhesive percentages did not seem to affect the material's attenuation properties. This suggests that the adhesive used in *Rhizophora* spp. does not introduce any impurities that could interfere with how the material interacts with radiation. The *Rhizophora* spp. samples showed steady attenuation values, ranging from 0.17 to 0.18 cm^2/g for ^{60}Co and 0.12 to 0.13 cm^2/g for ^{137}Cs, revealing that no heavy elements, such as lead or barium, were present. However, future studies should investigate the formulation of specific adhesives that might impact attenuation, especially because slight variations could arise. This further research would help refine the material's performance, ensuring it remains reliable for dosimetry and imaging in large-scale applications.

Previous work also demonstrates that dispersion and grain size of the added particulates may have a great impact on attenuation performance of the raw material–additives composite (Azeez *et al.* 2013). When particulates are not evenly dispersed, the resulting inhomogeneities can reduce the material's ability to attenuate radiation effectively. Such inconsistencies can negatively impact the overall capability of the composite. However, the consistency in attenuation coefficients observed in this work indicates that varying the adhesive percentages did not significantly influence the material's attenuation behavior. This suggests that the adhesive used with *Rhizophora* spp. neither alters the microstructural uniformity nor introduces impurities that could interfere with photon interactions, thereby maintaining the radiation attenuation properties of the composite regardless of adhesive concentration. Another study compared theoretical

values with computational evaluations of the attenuation properties of polymers and found that, although the actual results of these theoretically derived examples may vary, the discrepancies that are likely influenced by factors, such as material homogeneity, density, and impurities, are generally expected to remain minimal (Elmalı *et al.* 2025).

Elmalı *et al.* (2025) also highlighted that geometric modelling can be applied to estimate the expected performance of composites prior to production, allowing material savings while effectively representing system behaviour with minimal projection requirements (Elmalı *et al.* 2025). The study further emphasised the significant role of various computer programs in advancing materials science and supporting the evaluation of innovative approaches. Present work employs Monte Carlo simulations using the GATE platform to compute the linear and mass attenuation coefficients of the materials. Similar to geometric modelling, the Monte Carlo–based GATE (Sarrut *et al.* 2014; Langer *et al.* 2020; Karimipourfard *et al.* 2022; Sarrut *et al.* 2022; Sarrut *et al.* 2025) approach provides a cost-effective and reliable means to represent system behaviour, enabling accurate evaluation of radiation interaction without the need for extensive experimental trials. This highlights the broader importance of computational tools in materials research, where they not only reduce resource consumption but also offer precise insights into the attenuation properties of innovative composites.

CONCLUSIONS

1. The soy-lignin bonded *Rhizophora* spp. at particle size of 104 to 210 µm (Sample B) exhibited the lowest overall attenuation variation of 0.06 to 1.40%, with the addition of 6 and 12% adhesives, demonstrates that variations in adhesive content do not significantly influence the material's attenuation behaviour.
2. GATE emerges as potential computational tools in evaluating attenuation properties of developed materials especially in radiation study.

ACKNOWLEDGMENTS

The authors acknowledge the Fundamental Research Grant Scheme (FRGS/1/2024/STG07/UKM/02/4) from the Ministry of Higher Education (MOHE) and Universiti Kebangsaan Malaysia Geran Galakan Penyelidik Muda (GGPM-2023-027).

USE OF GENERATIVE AI

ChatGPT (GPT-5) was employed primarily for rephrasing sentences and elaboration to enhance clarity and readability, and for grammar checking to ensure linguistic accuracy in academic and professional writing.

REFERENCES CITED

Abd Hamid, P. N. K., Yusof, M. F. M., and Hashim, R. (2018). "Design and evaluation of corn starch-bonded *Rhizophora* spp. particleboard phantoms for SPECT/CT imaging," in: *IOP Conference Series: Materials Science & Engineering*, IOP Publishing, Bristol, UK, article 012041.

Abdalla, A. M., Al-Naggar, T. I., Bashiri, A. M., and Alsareii, S. A. (2022). "Radiation shielding performance for local granites," *Progress in Nuclear Energy* 150, article 104294. https://doi.org/10.1016/j.pnucene.2022.104294 https://www.sciencedirect.com/science/article/pii/S014919702200169X

Abdi, Z., Baghani, H. R., and Shamsabadi, R. (2025). "Evaluating the Kerma coefficients relevant to various water-equivalent materials at different photon energies," *Nuclear Engineering and Technology* 57(2), article 103174. https://doi.org/10.1016/j.net.2024.08.043 https://www.sciencedirect.com/science/article/pii/S1738573324004224

Almalki, H., Marashdeh, M. W., Alsuhybani, M.,and Almurayshid, M. (2024). "Evaluation of radiation attenuation properties of breast equivalent phantom material made of gelatin material in mammographic X-ray energies," *Journal of Radiation Research and Applied Sciences* 17(1), article 100817. https://doi.org/10.1016/j.jrras.2024.100817 https://www.sciencedirect.com/science/article/pii/S1687850724000013

Azeez, A. B., Mohammed, K. S., Abdullah, M. M., Hussin, K., Sandu, A. V., and Razak, R. A. (2013). "The effect of various waste materials' contents on the attenuation level of anti-radiation shielding concrete," *Mater. (Basel)* 6(10), 4836-4848. https://doi.org/10.3390/ma6104836

Benameur, Y., Tahiri, M., Mkimel, M., El Baydaoui, R., Najeh, M., Sahraoui, S., Benchekroun, N., Bougteb, M., El Hariri, B., and Mesradi, M. R. (2023). "Fetal dose estimation during pregnancy using Gate Monte Carlo simulation: Application of Hodgkin's lymphoma radiotherapy," *Radiat. Prot. Dosimetry* 199(7), 581-587. https://doi.org/10.1093/rpd/ncad057

Bradley, D. A., Tajuddin, A. A., Sudin, C. W. A. C. W., and Bauk, S. (1991). "Photon attenuation studies on tropical hardwoods," *Int. J. Radiat. Appl. Instrumentation. Part A. Appl. Radiat. Isot.* 42, 771-773.

Buyukyildiz, M. Kaur, P., Thakur, S., and Atlı, R. (2024). "Study of phantom materials close to 1 keV photon energy for radiation applications," *Radiation Physics and Chemistry* 215, article 111375. https://doi.org/10.1016/j.radphyschem.2023.111375 https://www.sciencedirect.com/science/article/pii/S0969806X23006217

Buvat, I., and Lazaro, D. (2006). "Monte Carlo simulations in emission tomography and GATE: An overview," *Nucl. Instrum. Methods Phys. Res., Sect. A* 569(2), 323-329. https://doi.org/10.1016/j.nima.2006.08.039

Elmalı, H. M., Martyn, E., and Baydoğan, N. (2025). "A theoretical study: Radiation shielding features of polymer materials," *CEUR Workshop Proceedings* 3970, 341-347.

İrem, E. R. K., Nesrin Altinsoy, Ş. İpek Karaaslan, and Ayçin Bora (2017). "Determination of photon mass attenuation coefficient for some phantom materials using GATE Code and comparison with experimental and XCOM data," *International Journal of Nuclear and Radiation Science and Technology* 2(1), article 28. https://doi.org/10.22399/ijsusat.28

Grevillot, L., Frisson, T., Maneval, D., Zahra, N., Badel, J.-N., and Sarrut, D. (2011). "Simulation of a 6 MV Elekta Precise LINAC photon beam using GATE/GEANT4," *Phys. Med. Biol.* 56(4), 903-918. https://doi.org/10.1088/0031-9155/56/4/002

Jan, S., Benoit, D., Becheva, E., Carlier, T., Cassol, F., Descourt, P., Frisson, T., Grevillot, L., Guigues, L., Maigne, L., *et al.* (2011). "GATE V6: A major enhancement of the GATE simulation platform enabling modelling of CT and radiotherapy," *Phys. Med. Biol.* 56(4), 881-901. https://doi.org/10.1088/0031-9155/56/4/001

Kanematsu, N., Koba, Y., and Ogata, R. (2013). "Evaluation of plastic materials for range shifting, range compensation, and solid-phantom dosimetry in carbon-ion radiotherapy," *Med. Phys.* 40(4), article 041724. https://doi.org/10.1118/1.4795338

Karimipourfard, M., Sina, S., and Alavi, M. S. (2022). "Toward three-dimensional patient-specific internal dosimetry using GATE Monte Carlo technique," *Radiation Physics and Chemistry* 195, article 110046.

Kaya, S. (2025). "Investigation of radiation shielding performance in borosilicate ceramic glass samples." *Bilecik Şeyh Edebali University Journal of Science* 12(2), 555-567. https://doi.org/10.35193/bseufbd.1666031

Khallouqi, A., A. Halimi, M. R. Mesradi, K. El Mansouri, and H. Sekkat. (2024). "Comparing tissue-equivalent properties of polyester and epoxy resins with PMMA material using Gate/Geant4 simulation toolkit," *Radiation Physics and Chemistry* 220, article 111702. https://doi.org/10.1016/j.radphyschem.2024.111702

Khoshhal, A. R., and Torshabi, A. E. (2024). "Feasibility of anthropomorphic head phantom design using DLP 3D printing for dosimetry," *Journal of Nuclear Research and Applications* 4(3), 24-32. https://doi.org/10.24200/jonra.2024.1634.1140

Langer, M., Cen, Z., Rit, S., and Létang, J. M. (2020). "Towards Monte Carlo simulation of X-ray phase contrast using GATE," *Optics Express* 28(10), 14522-14535.

Marashdeh, M., and Abdulkarim, M. (2023). "Determination of the attenuation coefficients of epoxy resin with carbopol polymer as a breast phantom material at low photon energy range," *Polymers (Basel)* 15(11), article 2645. https://doi.org/10.3390/polym15112645

Marashdeh, M. W., Bauk, S., and Tajuddin, A. A. (2012). "Measurement of mass attenuation coefficients of *Rhizophora* spp. binderless particleboards in the 16.59–25.26 keV photon energy range and their density profile using X-ray computed tomography," *Appl. Radiat. Isot.* 70(4), 656-662. https://doi.org/10.1016/j.apradiso.2012.01.008

McGarry, C. K., Grattan, L. J., Ivory, A. M., Leek, F., Liney, G. P., Liu, Y., Miloro, P., Rai, R., Robinson, A., Shih, A. J., *et al.* (2020). "Tissue mimicking materials for imaging and therapy phantoms: A review," *Phys. Med. Biol.* 65(23), article 23TR01. https://doi.org/10.1088/1361-6560/abbd17

Moradi, F., Khandaker, M. U., Alrefae, T., Ramazanian, H., & Bradley, D. A. (2019). "Monte Carlo simulations and analysis of transmitted gamma ray spectra through various tissue phantoms," *Applied Radiation and Isotopes* 146, 120-126. https://doi.org/10.1016/j.apradiso.2019.01.031 https://www.sciencedirect.com/science/article/pii/S0969804318307516

Nasr, B., Villa, M., Benoit, D., Visvikis, D., and Bert, J. (2024). "Monte Carlo dosimetry validation for X-ray guided endovascular procedures," *Ann. Vasc. Surg.* 99, 186-192. https://doi.org/10.1016/j.avsg.2023.07.104

Park, H., Paganetti, H., Schuemann, J., Jia, X., and Min, C. H. (2021). "Monte Carlo

methods for device simulations in radiation therapy," *Phys. Med. Biol.* 66, article 18TR01. https://doi.org/10.1088/1361-6560/ac1d1f

Sadoughi, H.-R., Nasseri, S., Momennezhad, M., Sadeghi, H.-R., and Bahreyni-Toosi, M.-H. (2014). "A comparison between GATE and MCNPX Monte Carlo codes in simulation of medical linear accelerator," *J. Med. Signals Sens.* 4(1), 10-17. https://doi.org/10.4103/2228-7477.128433

Samson, D., Shukri, A., Jafri, M. Z. M., Hashim, R., Aziz, M. Z. A., and Yusof, M. F. M. (2020a). "Tissue equivalent materials from SPC-SPI/NaOH/IA-PAE bonded mangrove wood characterized for radiation therapy dosimetry," *Sci. Proc. Ser.* 2, 115-120.

Samson, D. O., Mat Jafri, M. Z., Hashim, R., Sulaiman, O., Aziz, M. Z. A., and Yusof, M. F. M. (2020b). "*Rhizophora* spp. particleboards incorporating defatted soy flour bonded with NaOH/IA-PAE: Towards a water equivalent phantom material," *Radiat. Phys. Chem.* 176, article 109057. https://doi.org/10.1016/j.radphyschem.2020.109057

Samson, D. O., Shukri, A., Jafri, M. Z. M., Hashim, R., Sulaiman, O., Aziz, M. Z. A., and Yusof, M. F. M. (2020c). "Characterization of *Rhizophora* spp. particleboards with soy protein isolate modified with NaOH/IA-PAE adhesive for use as phantom material at photon energies of 16.59–25.26 keV," *Nucl. Eng. Technol.* 52(12), 2835-2843.

Samson, D. O., Shukri, A., Hashikin, N. A. A., Zuber, S. H., Aziz, M. Z., Hashim, R., Yusof, M. F., Rabaiee, N. A., and Gemanam, S. J. (2023). "Dosimetric characterization of DSF/NaOH/IA-PAE/*Rhizophora* spp. phantom material for radiation therapy," *Polymers (Basel)* 15(1), article 244. https://doi.org/10.3390/polym15010244

Sarrut, D., Arbor, N., Baudier, T., Borys, D., Etxebeste, A., Fuchs, H., Gajewski, J., Grevillot, L., Jan, S., Kagadis, G. C., *et al.* (2022). "The OpenGATE ecosystem for Monte Carlo simulation in medical physics," *Phys. Med. Biol.* 67(18), article 184001. https://doi.org/10.1088/1361-6560/ac8c83

Sarrut, D., Arbor, N., Baudier, T., Bert, J., Chatzipapas, K., Favaretto, M., Fuchs, H., Grevillot, L., Harb, H., *et al.* (2025). "GATE 10 Monte Carlo particle transport simulation-Part I: Development and new features," *Physics in Medicine and Biology 71*(1), article 015042. https://doi.org/10.1088/1361-6560/ae237b

Sarrut, D., Bardiès, M., Boussion, N., Freud, N., Jan, S., Létang, J.-M., Loudos, G., Maigne, L., Marcatili, S., Mauxion, T., *et al.* (2014). "A review of the use and potential of the GATE Monte Carlo simulation code for radiation therapy and dosimetry applications," *Med. Phys.* 41(6 Part 1), article 064301. https://doi.org/10.1118/1.4871617

Scalzetti, E. M., Huda, W., Bhatt, S., and Ogden, K. M. (2008). "A method to obtain mean organ doses in a Rando phantom," *Health Phys.* 95(2), 241-244. https://doi.org/10.1097/01.HP.0000310997.09116.e3

Silberstein, J., and Sun, Z. (2024). "Advances and applications of three-dimensional-printed patient-specific chest phantoms in radiology: A systematic review," *Appl. Sci.* 14(13), article 5467. https://doi.org/10.3390/app14135467

Stocken, T., Vanschoenwinkel, B., Carroll, D., Cavanaugh, K. C., and Koedam, N. (2022). "Mangrove dispersal disrupted by projected changes in global seawater density," *Nature Climate Change* 12(7), 685-691. https://doi.org/10.1038/s41558-022-01391-9

Sudin, C., Tajuddin, A. A., and Bradley, D. A. (1988). "Evaluation of tissue-equivalent

media for dosimetric studies," in: *Proceeding of Local Seminar Activities on Radiation Physics, Biophysics and Medical Physics*, Kuala Lumpur, Malaysia. pp. 71-80.

Thiam, C. O., Breton, V., Donnarieix, D., Habib, B., and Maigne, L. (2008). "Validation of a dose deposited by low-energy photons using GATE/GEANT4," *Phys. Med. Biol.* 53(11), 3039-3051. https://doi.org/10.1088/0031-9155/53/11/019

Tousi, E. T. (2022). "Monte Carlo simulation of the mass attenuation coefficient and effective atomic number of the *Eremurus–Rhizophora* spp. particleboard phantom at the mammography energy range," *Prog. Nucl. Energy* 149, article 104281. https://doi.org/10.1016/j.pnucene.2022.104281

Tousi, E. T., and Hamid, R. S. (2024). "Dosimetric evaluation of *Rhizophora* spp. particleboard bonded with animal protein adhesive at X-ray energies below 100 kVp," *Applied Radiation and Isotopes* 214, article 111538. https://doi.org/10.1016/j.apradiso.2024.111538

Yusof, M. F. M., and Fahmi, M. (2017). "Design and dosimetric evaluation of tannin-based *Rhizophora* spp. particleboards as phantoms for high energy photons and electrons," *J. Radiol. Sci.* 298, article 012038. https://doi.org/10.1088/1757899X/298/1/012038

Yusof, M. F. M., Abdullah, R., Tajuddin, A. A., Hashim, R., Bauk, S., and Hamid, P. N. K. A. (2018). "Design and dosimetric evaluation of tannin-based *Rhizophora* spp. particleboards as phantoms for high energy photons and electrons," in: *IOP Conference Series: Materials Science & Engineering*, IOP Publishing, Bristol, UK, article 012038.

Yusof, M. F. M., Hamid, P. N. K. A., Tajuddin, A. A., Hashim, R., Bauk, S., Isa, N. M., and Isa, M. J. M. (2017). "Mass attenuation coefficient of tannin-added *Rhizophora* spp. particleboards at 16.59–25.56 keV photons, and ^{137}Cs and ^{60}Co gamma energies," *Radiol. Phys. Technol.* 10, 331-339. https://doi.org/10.1007/s12194-017-0408-3

Zuber, S. H., Abdul Hadi, M. F. R., Hashikin, N. A. A., Mohd Yusof, M. F., and Aziz, M. Z. A. (2024a). "Attenuation coefficients of soy–lignin bonded *Rhizophora* spp. particleboard as a potential phantom material using Monte Carlo GATE," *BioResources* 19(1), 8920-8934. https://doi.org/10.15376/biores.19.1.8920-8934

Zuber, S. H., Abdul Hadi, M. F. R., Hashikin, N. A. A., Mohd Yusof, M. F., Aziz, M. Z. A., Hashim, R., Oluwafemi, S. D., and Isa, N. M. (2022a). "Estimation of linear and mass attenuation coefficients of soy–lignin bonded *Rhizophora* spp. particleboard as a potential phantom material using caesium-137 and cobalt-60," *Radiat. Environ. Biophys.* 61, 435-443. https://doi.org/10.1007/s00411-022-00978-2

Zuber, S. H., Hadi, M. F. R. A., Hashikin, N. A. A., Samson, D. O., Ishak, N. H., Raof, N. A., Aziz, M. Z. A., Yusof, M. F. M., and Rabaiee, N. A. (2025). "Dosimetric evaluation of brain radiotherapy using custom-made *Rhizophora* head phantom – Comparison between Monte Carlo GATE and treatment planning system MONACO," *Int. J. Radiat. Res.* 23, 13-20.

Zuber, S. H., Hadi, M. F. R. A., Oluwafemi, S. D., and Fahmi, M. (2022b). "Compton scattering study using Ludlum configuration for tissue-equivalent phantom material made from soy–lignin bonded *Rhizophora* spp. particleboard," *Sains Malays.* 51(6), 1895-1904. https://doi.org//10.17576/jsm-2022-5106-24

Zuber, S. H., Hashikin, N., Mohd Yusof, M. F., and Hashim, R. (2020). "Lignin and soy flour as adhesive materials in the fabrication of *Rhizophora* spp. particleboard for medical physics applications," *J. Adhes.* 98(5), 429-448

https://doi.org/10.1080/00218464.2020.1839430
Zuber, S. H., Yusof, M. F. M., Hashikin, N. A. A., Samson, D. O., Aziz, M. Z. A., and Hashim, R. (2021a). "*Rhizophora* spp. as potential phantom material in medical physics applications – A review," *Radiat. Phys. Chem.* 189, article 109731. https://doi.org/10.1016/j.radphyschem.2021.109731
Zuber, S. H., Hashikin, N. A. A., Yusof, M. F. M., Aziz, M. A. A., and Hashim, R. (2021b). "Influence of different percentages of binders on the physico- mechanical properties of *Rhizophora* spp. particleboard as natural-based tissue-equivalent phantom for radiation dosimetry applications," *Polymers* 31(11), article 1868. https://www.mdpi.com/2073-4360/13/11/1868
Zuber, S. H., Abdul Hadi, M. F. R., Hashikin, N. A., Yusof, M. F. M., and Aziz, M. Z. A. (2024b). "Rhizophora-based particleboard bonded with soy flour and lignin as potential phantom," *BioResources* 19(3), 5467-5482. DOI: 10.15376/biores.19.3.5467-5482

Article submitted: September 29, 2025; Peer review completed: December 20, 2025; Revised version received: January 22, 2026; Accepted: February 8, 2026; Published: February 20, 2026.
DOI: 10.15376/biores.21.2.3394-3416

APPENDIX

Appendix A lists the density and the elemental composition of each sample for this study.

S1 = A0
Sample 19B448 : d=1.0 g/cm^3 ; n 14

+mat: name =Na20 ; f = 0.06777
+mat: name =MgO ; f = 0.03056
+mat: name =Al2O3 ; f = 0.00303
+mat: name =SiO2 ; f = 0.01414
+mat: name = P2O5 ; f = 0.01095
+mat: name =SO3 ; f = 0.03501
+mat: name =Cl ; f = 0.19607
+mat: name =K2O ; f = 0.04936
+mat: name =CaO ; f = 0.53794
+mat: name =MnO ; f = 0.01262
+mat: name = Fe203 ; f = 0.02873
+mat: name =Br ; f = 0.00273
+mat: name =SrO ; f = 0.00868
+mat: name =Bi2O3 ; f = 0.00238

S2 = B0
Sample 19B449 : d=1.0 g/cm^3 ; n 13

+mat: name =Na2O ; f = 0.07156
+mat: name =MgO ; f = 0.03357
+mat: name =Al2O3 ; f = 0.00161
+mat: name =SiO2 ; f = 0.01120
+mat: name = P2O5 ; f = 0.01080
+mat: name =SO3 ; f = 0.03805
+mat: name =Cl ; f = 0.19580
+mat: name =K2O ; f = 0.05925
+mat: name =CaO ; f = 0.51866
+mat: name =MnO ; f = 0.01533
+mat: name = Fe203 ; f = 0.03645
+mat: name =Br ; f = 0.00206
+mat: name =SrO ; f = 0.00566

S3 = C0
Sample 19B450 : d=1.0 g/cm^3 ; n 15

+mat: name =Na20 ; f = 0.06355
+mat: name =MgO ; f = 0.03161
+mat: name =Al2O3 ; f = 0.00254
+mat: name =SiO2 ; f = 0.01381
+mat: name = P2O5 ; f = 0.01017

+mat: name =SO3 ; f = 0.03901
+mat: name =Cl ; f = 0.17705
+mat: name =K2O ; f = 0.05241
+mat: name =CaO ; f = 0.52744
+mat: name =MnO ; f = 0.00961
+mat: name = Fe203 ; f = 0.05678
+mat: name =CuO ; f = 0.00577
+mat: name =ZnO ; f = 0.00232
+mat: name =Br ; f = 0.00220
+mat: name =SrO ; f = 0.00574

S4 = A6
Sample 19B451 : d=1.0 g/cm^3 ; n 15

+mat: name =Na20 ; f = 0.04668
+mat: name =MgO ; f = 0.03112
+mat: name =Al2O3 ; f = 0.00172
+mat: name =SiO2 ; f = 0.00956
+mat: name = P2O5 ; f = 0.04360
+mat: name =SO3 ; f = 0.08974
+mat: name =Cl ; f = 0.13310
+mat: name =K2O ; f = 0.13971
+mat: name =CaO ; f = 0.45968
+mat: name =MnO ; f = 0.00619
+mat: name = Fe203 ; f = 0.01602
+mat: name =NiO ; f = 0.00402
+mat: name =ZnO ; f = 0.00194
+mat: name =Br ; f = 0.00140
+mat: name =SrO ; f = 0.00588

S5 = A12
Sample 19B452 : d=1.0 g/cm^3 ; n 16

+mat: name =Na20 ; f = 0.04813
+mat: name =MgO ; f = 0.03340
+mat: name =Al2O3 ; f = 0.00278
+mat: name =SiO2 ; f = 0.01767
+mat: name = P2O5 ; f = 0.06363
+mat: name =SO3 ; f = 0.11936
+mat: name =Cl ; f = 0.12537
+mat: name =K2O ; f = 0.20368
+mat: name =CaO ; f = 0.34160
+mat: name =MnO ; f = 0.00665
+mat: name =Fe2O3 ; f = 0.02587
+mat: name = NiO ; f = 0.00217
+mat: name =CuO ; f = 0.00322
+mat: name =ZnO ; f = 0.00218
+mat: name =Br ; f = 0.00068

+mat: name =SrO ; f = 0.00308

S6 = B6
Sample 19B453 : d=1.0 g/cm^3 ; n 13

+mat: name =Na20 ; f = 0.05774
+mat: name =MgO ; f = 0.03409
+mat: name =Al2O3 ; f = 0.00265
+mat: name =SiO2 ; f = 0.02115
+mat: name = P2O5 ; f = 0.03888
+mat: name =SO3 ; f = 0.08557
+mat: name =Cl ; f = 0.15321
+mat: name =K2O ; f = 0.14988
+mat: name =CaO ; f = 0.41897
+mat: name =MnO ; f = 0.00667
+mat: name = Fe203 ; f = 0.02703
+mat: name =ZnO ; f = 0.00159
+mat: name =Br ; f = 0.00260

S7 = B12
Sample 19B454 : d=1.0 g/cm^3 ; n 14

+mat: name =Na20 ; f = 0.05231
+mat: name =MgO ; f = 0.03277
+mat: name =Al2O3 ; f = 0.00210
+mat: name =SiO2 ; f = 0.01411
+mat: name = P2O5 ; f = 0.05087
+mat: name =SO3 ; f = 0.10721
+mat: name =Cl ; f = 0.11860
+mat: name =K2O ; f = 0.18101
+mat: name =CaO ; f = 0.39271
+mat: name =MnO ; f = 0.00796
+mat: name = Fe203 ; f = 0.03439
+mat: name =ZnO ; f = 0.00118
+mat: name =Br ; f = 0.00130
+mat: name =SrO ; f = 0.00349

S8 = C6
Sample 19B455 : d=1.0 g/cm^3 ; n 16

+mat: name =Na20 ; f = 0.05036
+mat: name =MgO ; f = 0.02771
+mat: name =Al2O3 ; f = 0.00296
+mat: name =SiO2 ; f = 0.01745
+mat: name = P2O5 ; f = 0.03598
+mat: name =SO3 ; f = 0.08413
+mat: name =Cl ; f = 0.12947
+mat: name =K2O ; f = 0.14883

+mat: name =CaO ; f = 0.42740
+mat: name =MnO ; f = 0.00788
+mat: name =Fe2O3 ; f = 0.04926
+mat: name = ZnO ; f = 0.00195
+mat: name =SeO2 ; f = 0.00149
+mat: name =Br ; f = 0.00101
+mat: name =SrO ; f = 0.00332
+mat: name =Nd2O3; f = 0.01081

S9 = C12
Sample 19B456 : d=1.0 g/cm^3 ; n 15

+mat: name =Na20 ; f = 0.04708
+mat: name =MgO ; f = 0.02832
+mat: name =Al2O3 ; f = 0.00200
+mat: name =SiO2 ; f = 0.01428
+mat: name = P2O5 ; f = 0.04456
+mat: name =SO3 ; f = 0.10235
+mat: name =Cl ; f = 0.11623
+mat: name =K2O ; f = 0.18399
+mat: name =CaO ; f = 0.40319
+mat: name =MnO ; f = 0.00633
+mat: name = Fe203 ; f = 0.04425
+mat: name =ZnO ; f = 0.00190
+mat: name =Br ; f = 0.00104
+mat: name =SrO ; f = 0.00280
+mat: name =PtO2 ; f = 0.00169